Journal of King Saud University - Computer and Information Sciences 36 (2024) 101944

HOSTED BY

Contents lists available at ScienceDirect

Journal of King Saud University - Computer and Information Sciences

journal homepage: www.sciencedirect.com

Automatic melanoma detection using discrete cosine transform features and metadata on dermoscopic images

Shamim Yousefi [a], Samad Najjar-Ghabel [a,*], Ramin Danehchin [b], Shahab S. Band [c,***], Chung-Chian Hsu [c], Amir Mosavi [d,e,**]

[a] Department of Computer Engineering, University of Mohaghegh Ardabili, Ardabil, Iran
[b] Faculty of Electrical and Computer Engineering, University of Tabriz, Tabriz, Iran
[c] International Graduate School of Artificial Intelligence, National Yunlin University of Science and Technology, Douliu, Taiwan, ROC
[d] John von Neumann Faculty of Informatics, Budapest, Hungary
[e] Ludovika University of Public Service, Budapest, Hungary

ARTICLE INFO

Keywords:
Dermoscopic image
Discrete cosine transform features
Melanoma detection
Metadata
Artificial intelligence
Machine learning
Data science
Big data

ABSTRACT

Machine learning contributes in improving the accuracy of melanoma detection. There are extensive studies in classic and deep learning-based approaches for melanoma detection in the literature. Still, they are not accurate or require high learning data. This paper proposes a hybrid mechanism for automated melanoma detection on dermoscopic images based on Discrete Cosine Transform features and metadata. It is composed of three steps. First, extra information/artifacts are deleted; the remaining pixels are standardized for accurate processing. Second, the reliability of the mechanism is improved by the Radon transform, extra data is removed using the Top-hat filter, and the detection rate is increased by Discrete Wavelet Transform and Discrete Cosine Transform. Then, the number of features is reduced by Locality Sensitive Discriminant Analysis. The third step divides the images into learning and test ones to create image-based models using learning data. Finally, the best model is selected based on test data and improved by a metadata-based model. Simulation results show that the decision tree provides the most practical image-based model by improving accuracy and sensitivity. Besides, the comparison results demonstrate that our model improves the F-Value to detect melanoma superior to other approaches.

1. Introduction

Cutaneous melanoma, commonly referred to as "melanoma," stands as the most aggressive form of skin cancer, often leading to successive metastases and associated with a high mortality rate (Adegun and Viriri, 2021; Khan et al., 2022; Magalhaes et al., 2021; Mirikharaji et al., 2023). Globally, the number of melanoma patients has surged rapidly, with more than 250,000 melanoma cases and 500,000 non-melanoma skin cancers reported in 2020 alone, as per the World Health Organization (Alheejawi et al., 2021; Wang et al., 2021).

Melanoma typically presents as raised dark lesions, although some malignant tumors lack dark pigment and manifest as white, pink, or tan flat lesions (Huang et al., 2021). Additionally, features such as the existence and texture of structures complicate the distinction between cutaneous and benign lesions, making the process time-consuming (Thiyaneswaran et al., 2021; Wang et al., 2023). Timely intervention in the early stages of skin lesion development is crucial, preventing the spread of melanoma through blood and lymphatic vessels (Hou et al., 2021). Thus, it is crucial to exploit various visual inspections for the early diagnosis of melanoma. Dermoscopy is a standard tool for early melanoma detection (Gareau et al., 2020; Wang et al., 2022). It magnifies the skin images, evaluates the pigmented lesions, increases the clarity of abnormal structural features, and accurately observes the border of the lesions without the need for a biopsy (Daghrir et al., 2020). However, despite its utility, dermoscopy presents challenges, as experts often struggle to achieve acceptable performance in melanoma

* Corresponding author at: University of Mohaghegh Ardabili, Ardabil, Iran.
** Co-Corresponding author at: Obuda University, Hungary.
*** Co-Corresponding author at: National Yunlin University of Science and Technology, Douliu, Taiwan, ROC.
E-mail addresses: Sh.yousefi@uma.ac.ir (S. Yousefi), S.Najjar@uma.ac.ir (S. Najjar-Ghabel), R.danehchin00@gmail.com (R. Danehchin), shahab@yuntech.edu.tw (S.S. Band), hsucc@yuntech.edu.tw (C.-C. Hsu), amir.mosavi@uni-obuda.hu (A. Mosavi).

https://doi.org/10.1016/j.jksuci.2024.101944
Received 9 September 2023; Received in revised form 27 December 2023; Accepted 22 January 2024
Available online 1 February 2024

detection on raw dermoscopic images (Patil and Bellary, 2020; Zhou et al., 2022). Machine learning-based image analysis approaches have proven effective in addressing these challenges, offering quick and accurate detection of skin abnormalities on dermoscopic images (Pereira et al., 2022; Thiyaneswaran et al., 2021; Yousefi et al., 2020).

Several automated approaches for melanoma detection exist in the literature, employing classic machine learning algorithms such as Support Vector Machine (SVM), Random Forest, K-Nearest Neighbor (K-NN) (Eman et al., 2023), and Artificial Neural Network (ANN) (Efimenko et al., 2020; Eliwa et al., 2023; Kassem et al., 2021). However, these classic algorithms, while practical, often fall short in medical applications due to the lack of pre-processing steps to eliminate noise and their reliance on binary classifiers (Ningrum et al., 2021). To address these challenges, deep learning-based approaches, such as Convolutional Neural Networks (CNNs), have been proposed, offering high accuracy but demanding extensive training data and training time (Wu et al., 2020). At the same time, the main objective of healthcare applications is to maximize detection accuracy using a minimum number of training data (Yousefi et al., 2020).

This paper proposes a novel mechanism for automated melanoma detection using Discrete Cosine Transform (DCT) features (Acharya et al., 2017) on dermoscopic images. The proposed Automated Melanoma Detection (AMD) mechanism consists of three primary steps. The first step involves the removal of patient information and hair artifacts, with the remaining pixels standardized for high resolution and precise processing. In the second step, the reliability of AMD is enhanced through the Radon transform (Ziou et al., 2021), the removal of noise using the Top-hat filter (Ramos-Soto et al., 2021), and increased detection rates using Discrete Wavelet Transform (DWT) (Shajahan et al., 2021) and DCT features. Then, the extracted 2D coefficients are converted to the 1D vector using the Zigzag approach (Wang and Chen, 2021), and the number of final features is reduced using the Locality Sensitive Discriminant Analysis (LSDA) (Yao et al., 2020). The third step categorizes processed images into training and test data, with training data used to create different models for automated melanoma detection and test data evaluating the models to select the best image-based model. Additionally, a metadata-based model is introduced to enhance the image-based model's performance using sex, rash site, and age as key features.

Simulation analysis of image-based models reveals that the Decision Tree (DT) (Lu and Ma, 2020) classifies dermoscopic images more accurately and sensitively than other classifiers (K-NN and SVM), improving the harmonic mean of sensitivity and accuracy. DT outperforms other classifiers by minimizing cross-validation errors. Furthermore, comparison results demonstrate that the proposed image and metadata-based hybrid model outperforms other state-of-the-art approaches in melanoma detection on dermoscopic images, enhancing the F-Value.

The fundamental contributions of our paper are summarized as the following:

- Developing a novel image and metadata-based hybrid mechanism for automated melanoma detection with maximum accuracy and minimum training data.
- Improving the detection rate using DWT and DCT features.
- Reducing the number of features using LSDA.
- Exploiting different classifiers to extract the most accurate, precise, and sensitive image-based model with minor cross-validation errors.
- Introducing a metadata-based model to improve the performance of the image-based one using sex, rash site, and age as the main features.

The rest of the paper is organized as follows: Section 2 offers a comprehensive literature review, delving into existing research in the field. In Section 3, we detail the proposed AMD mechanism, outlining its various components and processes. Section 4 is dedicated to the discussion of simulation results, providing insights into the model's performance. Section 5 encompasses a thorough exploration of the limitations and a discussion of the proposed model. Finally, Section 6 serves as the conclusion, summarizing key findings and potential avenues for future research.

2. Related work

Melanoma, a life-threatening skin cancer, necessitates early detection. The literature presents a diverse array of machine learning-based automated approaches to tackle this challenge (Abbes et al., 2021; Gálvez et al., 2021; Murugan et al., 2019). These approaches are categorized into classic and deep learning-based automated melanoma detection.

In the realm of classic melanoma detection, Gálvez et al. (2021) have proposed an image processing-based method to segment macroscopic skin images. It employs a filtering strategy to remove noise, hair, and artefacts, enhances pixels using morphological operators, separates tumour-affected skin through clustering-based binary approaches, extracts border points using discretization, and reconstructs a curve using a tailored functional network. While visual results support the suitability of the clustering-based approach, detailed analysis reveals low accuracy and reliance on a binary classifier for melanoma border detection on dermoscopic images.

Murugan et al. (2019) have presented another classic melanoma detection model based on SVM, Random Forest (Bai et al., 2022), and K-NN classifiers for detecting melanocytes in the epidermis. The model implements the watershed segmentation mechanism for image segmentation, utilizing the resulting segments for shape, asymmetry, border, colour, differential (ABCD) rule, and GLCM feature extraction (Saabia et al., 2019). Numerical results confirm that the SVM provides the best outcomes for skin cancer classification. Abbes et al. (2021) have employed the K-NN classifier to expedite early melanoma detection based on ontology, focusing on the ABCD rule for fuzzy lesion classification. While classic machine learning algorithms enhance sensitivity and accuracy in extracting features from dermoscopic images, they lack a pre-processing step to eliminate noise.

Finally, Tumpa and Kabir (2021) have adopted a practical design of ANN for melanoma lesion detection on dermoscopic images. It enhances pixels with the Maximum Gradient Intensity (MGI) pre-processing algorithm (Chakkaravarthy and Chandrasekar, 2020), separates skin lesions from the background using Otsu thresholding segmentation, and calculates ABCD, GLCM, and LBP features (Kurdi et al., 2022) for accurate ANN-based detection. Despite achieving high accuracy on the ISIC dataset (Cassidy et al., 2022), the ANN-based approach falls short of optimal results after training.

To address the limitations of classic algorithms, some literature suggests deep learning-based approaches for melanoma detection on dermoscopic images (Doms et al., 2021; KUMAR TIWARI et al., 2021; Nawaz et al., 2022). In the case of deep learning-based models, Szegedy et al. (2015) have introduced a deep Convolutional Neural Network (CNN)-based architecture for image classification and detection in the ImageNet Large-Scale Visual Recognition Challenge 2014. It improves network depth and computing resource utilization using the Hebbian theory (Lagani et al., 2022) and the intuition of multi-scale processing. Raza et al. (2021) have proposed a classification framework using various pre-trained models and fine-tuned CNN-based transfer learning for ensemble detection. Abbas et al. (2021) have presented present an end-to-end deep learning-based framework utilizing data augmentation and a 7-layered CNN-based transfer learning for melanoma detection. It employs weights from the pre-trained ResNet-18 (Jing et al., 2021) and AlexNet (Lu et al., 2021) models and replaces the last layers of the network with some dense ones. The experiments indicate the promising results of deep learning-based approaches for melanoma detection on dermoscopic images. Finally, Cassidy et al. (2022) have trained widely-used deep learning architectures on ISIC datasets and removed duplicate

data, providing a noise-free CNN-based model. Although achieving high accuracy, CNN-based melanoma detection approaches require substantial training data.

To overcome the challenge of limited training data, Gajera et al. (2021) have used a CNN-based deep learning approach, extracting visual features from a pre-trained model and using classifiers for skin lesion classification. The results confirm the significance of boundary localization and cropping for relevant feature extraction in automated melanoma detection. However, a CNN with multiple layers demands extensive training time without a robust graphics processing unit.

In-depth analysis reveals that while classic algorithms are reasonably practical, they fall short in medical applications due to the absence of pre-processing steps and reliance on binary classifiers. Deep learning algorithms, although accurate, demand significant training data and training time. Meanwhile, the primary goal in healthcare applications is to maximize detection accuracy using a minimal amount of training data. The summary of methodologies, results, and the dataset size of the reviewed melanoma detection approaches are shown in Table 1.

Table 1
A comparison of melanoma detection approaches on dermoscopic images (methodologies, results, and the dataset sizes).

Paper	Methodology	Results	Dataset size
Gálvez et al. (2021)	Morphological operators (dilation and erosion), and NURBS functional network	Absolute error, and Relative error	Sample data of University Medical Center Groningen 2015 (160 dermoscopic images (Training: 45, and Test: 125))
Murugan et al. (2019)	K-NN, Random Forest, and SVM	Accuracy, Sensitivity, and Specificity	ISIC 2017 (1000 samples)
(Abbes et al. (2021)	Fuzzy decision rule-based K-NN	Accuracy, Sensitivity, and Specificity	Dermatology Information System 2012 and DermQuest 2012 (206 skin lesion images, 87 are not melanoma and 119 are melanoma)
Tumpa and Kabir (Tumpa and Kabir, 2021)	Maximum Gradient Intensity algorithm, ANN, and Otsu Thresholding algorithm	Accuracy, Sensitivity, Precision, and Specificity	ISIC 2020 (3600 images of malignant and benign lesions, with both training and testing data) and Ph2 (a total of 200 (160 benign and 40 malignant) data)
Raza et al. (2021)	CNN	Accuracy, Sensitivity, and Specificity	Acral melanoma and benign data set 2021 (724 dermoscopy images (506 images for training, 72 images for validation and 146 images for test set))
Cassidy et al. (2022)	CNN	Accuracy, Recall, and Precision	ISIC 2016 (Total: 1279, Training: 900, and Test: 379), ISIC 2017 (Total: 2600, Training: 2000, and Test: 600), ISIC 2018 (Total: 11527, Training: 10015, and Test: 1512), ISIC 2019 (Total: 33569, Training: 25331, and Test: 8238), ISIC 2020 (Total: 44108, Training: 33126, and Test: 10982)
Gajera et al. (2021)	Deep CNN	Accuracy, Sensitivity, Precision, and Specificity	Ph2 (a total of 200 (80 normal and 120 melanoma) data – a 70:30 ratio for training and testing)

3. AMD mechanism

This section introduces a machine learning-based mechanism designed for the automated detection of melanoma in dermoscopic images, referred to as Automated Melanoma Detection (AMD). As illustrated in Fig. 1, AMD encompasses three sequential steps: pre-processing, main processing, and classification. In the initial step, patient information and hair artifacts are removed from the raw dermoscopic images. The remaining pixels undergo standardization to achieve high resolution and enhance the accuracy of subsequent processing. Moving to the second step, the proposed mechanism's reliability is fortified by eliminating white (zero) noise through the Radon transform. Additionally, irrelevant data is filtered out using the Top-hat filter, and the detection rate is augmented by incorporating DWT and DCT features. The 2D DCT coefficients are then transformed into a 1D format using the Zigzag approach, and the number of final features is streamlined through LSDA. In the third step, the processed images are categorized into two groups: training and test. Various models are generated using the training data. Subsequently, these models are assessed based on test data, and the most effective one is chosen as the image-based model. Finally, the metadata-based model enhances the performance of the image-based one using sex, rash site, and age as primary features.

3.1. Pre-processing

The initial step of AMD is designed to enhance dermoscopic images, optimizing the efficiency of melanoma detection. This involves the removal of patient-specific information from the raw images, isolating only the suspected skin area. Subsequently, an artifact removal algorithm based on morphological filters is employed to extract hair artifacts. This algorithm identifies the positions of the hair artifacts and replaces them with neighboring pixels (Benyahia et al., 2022). Following this, the pixels, now devoid of hair artifacts, undergo standardization to achieve high resolution and facilitate more accurate processing in the subsequent step.

Moreover, contrast enhancement is applied to the standardized images using Contrast Limited Adaptive Histogram Equalization (CLAHE) (Mohd-Isa et al., 2021). This technique involves dividing the resized images into windows of specified sizes, enabling the synchronization of an adaptive histogram. Consequently, pixel intensities are substituted with new values to align with the intensity histogram values of each window. Fig. 2 illustrates resized dermoscopic images depicting healthy and melanoma-suffering skin after undergoing these enhancement processes.

3.2. Main processing

During this phase, the core processing steps of AMD are applied to the resized dermoscopic images. This encompassing process involves a series of stages, namely the Radon transform, Top-hat filter, DWT, DCT, Zigzag, and LSDA.

The efficacy of AMD is first bolstered through the application of the Radon transform, which serves to mitigate white (zero) noise. Simultaneously, the Top-hat filter is employed to eliminate superfluous data, enhancing the overall detection rate through the integration of DWT and DCT features. Subsequently, the 2D DCT coefficients are converted into a 1D format utilizing the Zigzag approach. Furthermore, the number of final features is streamlined by leveraging LSDA.

The ensuing sections provide a comprehensive description of each of these main processing phases.

3.2.1. Radon transform

In healthcare applications focused on detecting skin diseases, the

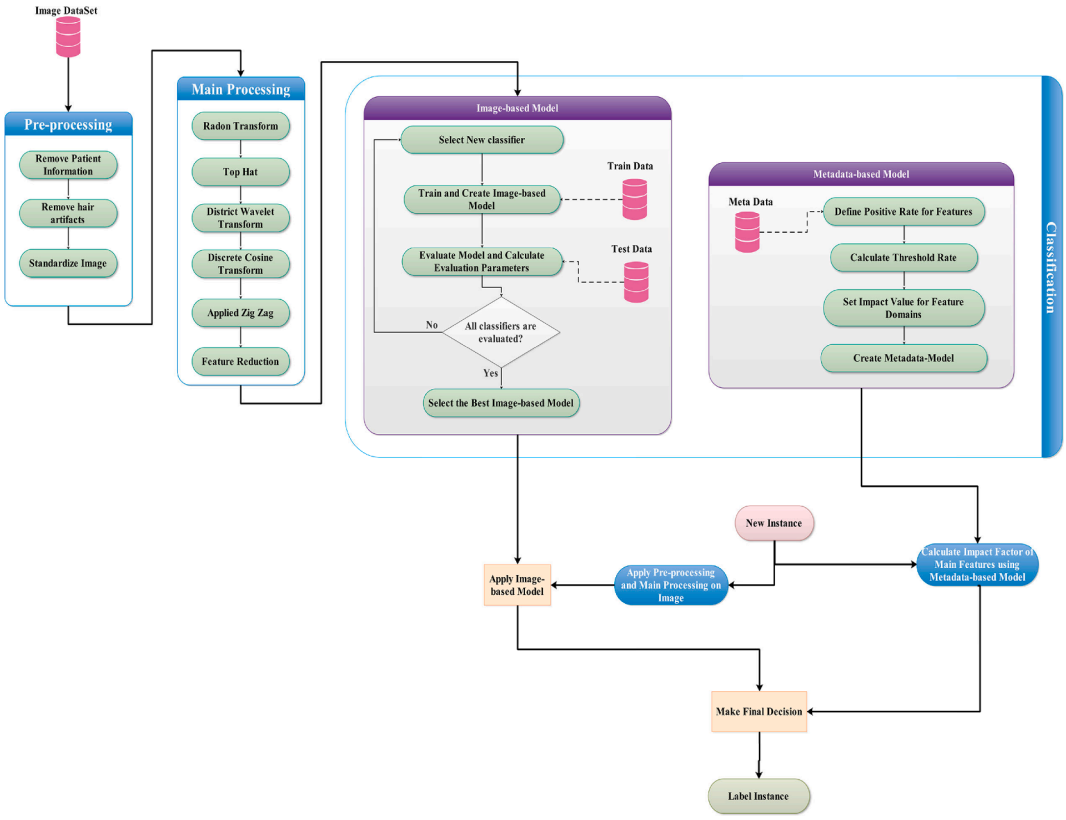

Fig. 1. The overall scheme of the AMD mechanism.

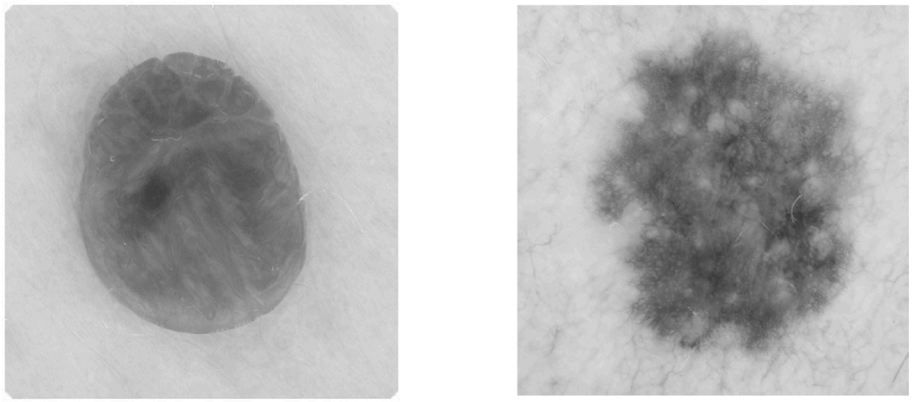

Fig. 2. Resized dermoscopic images: (a) healthy and (b) melanoma-suffering skins.

application of the Radon transform to resized dermoscopic images proves beneficial in enhancing practical reliability by mitigating white (zero) noises. The 2D Radon transform function is expressed as (1) (Ziou et al., 2021):

$$Rf(L) = \int_L f(x)|dx| \tag{1}$$

where the straight line L is parameterized based on the arc length z as given by (2) (Ziou et al., 2021):

$$(x(z), y(z)) = ((z\sin\alpha + s\cos\alpha), (-z\cos\alpha + s\sin\alpha)) \tag{2}$$

where s represents the distance between L and its normal vector angle with the x-axis. The coordinates (α, s) are also regarded as on-lines coordinates in 2D space. Radon transforms in these coordinates are calculated as expressed in (3) (Ziou et al., 2021):

$$Rf(\alpha, s) = \int_{-\infty}^{\infty} f(x(z), y(z))dz = \int_{-\infty}^{\infty} f((z\sin\alpha + s\cos\alpha), (-z\cos\alpha + s\sin\alpha))dz \tag{3}$$

The output of the 2D Radon transform on resized dermoscopic images is visually represented in Fig. 3.

3.2.2. Top-hat filter

The output of the Radon transform serves as the input for the Top-hat filter phase. The Top-hat filter is applied to the transformed dermoscopic images to eliminate redundant data. The primary process of the Top-hat filter includes two filters based on changes in the function of structural elements:

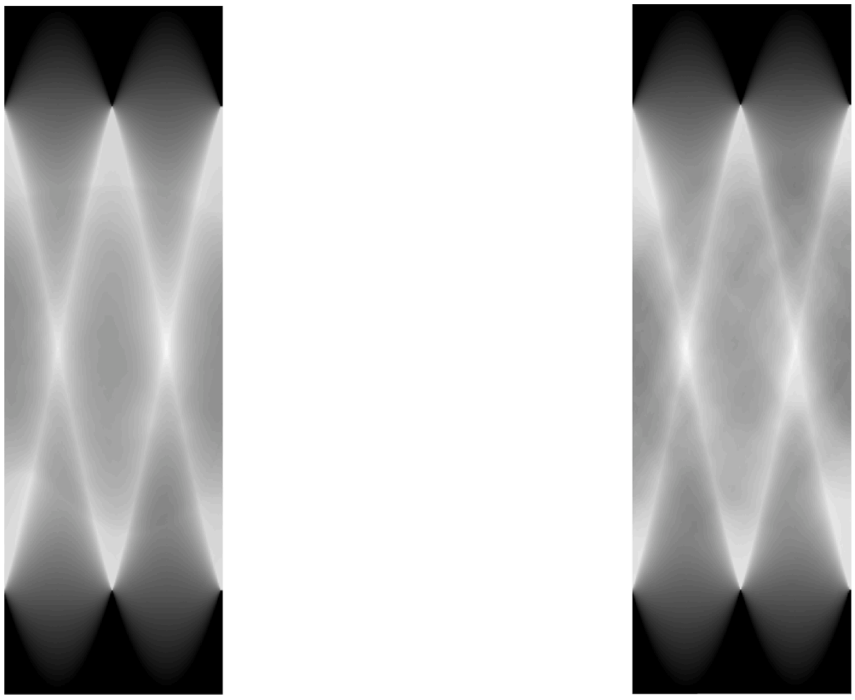

Fig. 3. 2D Radon transform on resized images: (a) healthy and (b) melanoma-suffering skins.

- The black Top-hat filter extracts dark structures from dermoscopic images.
- The white Top-hat filter extracts light structures from dermoscopic images.

The application of the Top-hat filter enhances the skin disease detection process on dermoscopic images. It amplifies the slope between light and dark pixels in transformed images, effectively removing excess pixels. Consequently, the edges of pixels are accentuated. The output of the Top-hat filter applied to transformed dermoscopic images is illustrated in Fig. 4.

3.2.3. Discrete wavelet transform

At this juncture, DWT is applied to the pixels obtained from the Top-hat filter to achieve a heightened detection rate. DWT proves effective in detecting abrupt changes in signal coefficients based on their structure. The outcomes of DWT on filtered images result in separate horizontal, vertical, and diagonal coefficients through the application of high-pass and low-pass filters. Fig. 5 provides a visual representation of DWT results on filtered dermoscopic images.

Fig. 4. Top-hat filter on transformed images: (a) healthy and (b) melanoma-suffering skins.

Fig. 5. DWT on filtered images: (a) healthy and (b) melanoma-suffering skins.

3.2.4. Discrete cosine transform

The DWT coefficients serve as the input to the DCT function for extracting frequency domain properties. DCT, known as an image compression method, facilitates the extraction of the frequency domain property matrix. It's worth noting that DCT properties enable more accurate detection of coefficients compared to DWT ones. The output of the DCT function applied to DWT coefficients is depicted in Fig. 6.

3.2.5. Zigzag

In this phase, a restricted set of DCT coefficients is chosen, and others are omitted. The selection of coefficients from the DCT matrix is a pivotal stage in feature extraction for melanoma detection. Our proposed mechanism leverages the Zigzag approach to convert 2D DCT coefficients into a 1D array. Zigzag integrates the coefficients by arranging them from the top-left element in a 1D matrix.

3.2.6. Locality sensitive discriminant analysis

In the final phase of the main processing, LSDA is employed to reduce the dimensions of the 1D coefficients obtained from DCT. It determines the classes and data correlation. LSDA assumes n data $X1, X2, \ldots, Xn \in R$, are random samples of M different types. Class compactness (Cc) and between-Class separability (Cs) for reducing data dimensions are calculated as presented in (4) and (5), respectively (Yao et al., 2020):

$$C_c = \min \sum_{lm} (k_1 - k_m)^2 W_{c,lm} \tag{4}$$

$$C_s = \min \sum_{lm} (k_1 - k_m)^2 W_{s,lm} \tag{5}$$

where $k_1 = \alpha^T X_1$ and $k_m = \alpha^T X_m$ are the 1D mappings of X_1 and X_m, while W_c and W_s denote the within-class and between-class separability weight matrices, respectively. The vector α signifies the predicted data direction.

population of more than two classes; if the difference exceeds a predetermined threshold, the feature is considered a significant attribute (Scott et al., 2020). Analysis of variance also calculates feature ranking, where the feature with the highest F-value is assigned the first rank.

3.3. Classification

The third step of AMD is designed to create the final model using the processed images and metadata, comprising image-based and metadata-based model phases. In the image-based model phase, various models are generated using training images, and their performance is evaluated based on tests to determine the best model as the output. In the metadata-based model phase, a positive rate is defined for all features, the threshold rate is calculated, and the impact value for various feature domains is set to create an appropriate metadata-based model. The classification phases are detailed below.

3.3.1. Image-based model

Following the pre-processing and main processing steps applied to all dermoscopic images (as shown in Fig. 1), output pixels are categorized into training and test images. Various classification algorithms, including DT, K-NN, and SVM, are executed on the training data to create the image-based model. The models are then evaluated using test data, and the best-performing model is selected as the output of the image-based model phase. The output for each image is either classified as healthy with an Image-based Model Impact Factor of zero ($IF_{IM} = 0$) or melanoma-suffering images with $IF_{IM} = 1$.

The proposed mechanism leverages the following classification algorithms:

Fig. 6. DCT on DWT coefficients: (a) healthy and (b) melanoma-suffering skins.

- *DT* is a common data mining algorithm in healthcare applications, particularly for skin disease detection from processed dermoscopic images. It is defined as a predictive model for classification-based applications, addressing erroneous datasets, and missing values, and utilizing nonparametric methods.
- *K-NN* is a simple classification approach with competitive results compared to similar algorithms. Its ease of interpretation, high predictivity, and acceptable computational time make K-NN widely used in healthcare applications, such as melanoma detection in processed dermoscopic images.
- *SVM* is a robust classification algorithm providing a richer model for sensitive data classification, especially in medical images, when used in combination with other machine learning tools. It is a suitable option for applications requiring high predictivity.

3.3.2. Metadata-based model

The metadata-based model phase aims to enhance the performance of the image-based one by incorporating key features. Sex, rash site, and age are considered the main features of the metadata-based model.

Given that men are more susceptible to melanoma than women (Benyahia et al., 2022), the first feature (sex) is divided into two categories: males with a moderate probability of melanoma and females with a low probability of melanoma. Additionally, a detailed examination of the patient's skin reveals that the rash site influences the risk of melanoma (Benyahia et al., 2022). Therefore, the second feature (rash site) is grouped into three categories: head, neck, oral, and genital with a high probability of melanoma, upper extremity with a moderate probability, and lower extremity, palms, soles, and torso with a low probability. Lastly, like any disease, age impacts the risk of developing melanoma in the human body. Hence, the third feature (age) is classified into four categories: 0–10 with a very low probability, 10–55 with a low probability, 55–60 with a moderate probability, 65–75 with a high probability, and 75–90 with a very high probability of melanoma. Finally, the Positive Rate (PR) for all features is calculated to indicate the percentage of melanoma-suffering images in each category.

At this juncture, the Threshold of Positive Rate (ToPR) for the dataset is defined as (6):

$$ToPR = \frac{Totalpositiverate(Melanoma - sufferingimages)}{TotalNumberofImage} \times 100 \quad (6)$$

It should be noted that ToPR serves as a pre-determined threshold to establish the Impact Factor (IF) of features in distinguishing between healthy and melanoma-suffering images. Algorithm 1 outlines the proposed procedure for determining the impact factor of features. The algorithm takes ToPR and the PR of the desired feature as inputs to calculate its IF, which improves the performance of the melanoma detection model. The algorithm specifies the IF value based on the PR range and returns it according to the following criteria:

1. If the PR of a feature is zero, its IF will be zero (very low).
2. If the PR of a feature is in the range of (0, ToPR], its IF will be 0.25 (low).
3. If the PR of a feature is in the range of (ToPR, 1.5 × ToPR], its IF will be 0.5 (medium).
4. If the PR of a feature is in the range of (1.5 × ToPR, 3 × ToPR], its IF will be 0.75 (high).
5. If the PR of a feature is higher than 3 × ToPR, its IF will be 1 (very high).

Algorithm 1: Setting the impact factor of features

Input: ToPR, PR // *Threshold of Positive Rate, and Positive Rate*
Output: IF // *Impact Factor*
Begin
  if (PR == 0)
    IF = 0 // *very low*
  else if (0 < PR ≤ ToPR)
    IF = 0.25 // *low*
  else if (ToPR < PR ≤ 1.5 × ToPR)
    IF = 0.5 // *medium*
  else if (1.5 × ToPR < PR ≤ 3 × ToPR)
    IF = 0.75 // *high*
  else if (PR ≥ 3 × ToPR)
    IF = 1 // *very high*
  return **IF**
End

In the final stage of metadata-based modelling, the Decision Value (DV) for distinguishing healthy and melanoma-suffering images is calculated as (7):

$$DV = IF_{IM} \times W_0 + IF_{Sex} \times W_1 + IF_{Age} \times W_2 + IF_{Site} \times W_3 \quad (7)$$

where IF_{IM}, IF_{Sex}, IF_{Age}, and IF_{Site} are the impact factors of the image-based model, sex, age, and rash site features, respectively. Besides, W_0, W_1, W_2, and W_3 represent the impact coefficients of the decision criteria.

Finally, the value of DV is assessed using (8) to make a Final Decision (FD):

if $(DV > \text{Threshold}_{Main})$

$\text{FD} = 1$; //Melanoma-suffering

else

$\text{FD} = 0$; *//Healthy* (8)

This means that if the calculated DV exceeds the predetermined (Threshold_{Main}), the FD value will be zero, indicating that the image is considered to depict melanoma. Conversely, if DV is less than or equal to the threshold, the FD value will be one, signifying that the image is categorized as healthy. It's important to note that determining the appropriate value for Threshold_{Main} involves tuning according to the desired performance criteria for the specific dataset.

4. Performance evaluation

This section assesses the performance of AMD and compares it with recent state-of-the-art melanoma detection mechanisms on dermoscopic images. The evaluation is conducted on the ISIC 2020 dataset (Cassidy et al., 2022), designed to advance research in automated Computer-Aided Diagnosis (CAD)-based melanoma/cancer detection. It refers to the International Skin Imaging Collaboration (ISIC) dataset for the year 2020 that is commonly used in the field of dermatology and machine learning for research on skin diseases, particularly melanoma detection using dermoscopic images.

The ISIC 2020 dataset contains a collection of dermoscopic images of skin lesions, including both malignant melanomas and benign moles or lesions with visual characteristics such as color, texture, shape, and other relevant information for skin disease analysis. These images serve as valuable resources for developing and evaluating algorithms and models for automated skin disease diagnosis, especially melanoma detection. It comprises a total of 1500 dermoscopic images in the training set (500 melanoma and 1000 healthy) and 174 dermoscopic images in the test set (84 melanoma and 90 healthy). The overall number of dermoscopic images is 33,125 (with 1674 images utilized for creating the image-based model). The details of ISIC 2020 training and test sets are shown in Table 2.

As outlined in Section 3.1, the pre-processing step eliminates patient information and hair artifacts from the images. Subsequently, it standardizes their sizes to 480 × 480 pixels to ensure uniform application of the main processing phases to all data. Moreover, AMD employs k-fold

Table 2
Details of ISIC 2020 training and test sets.

	Training Set	Test Set	Total
Melanoma	500	84	584
Healthy	1000	90	1090
Total	**1500**	**174**	**1674**

cross-validation (with k = 10) in statistical data analysis to assess the generalizability and training data independence of the model (Kaminsky et al., 2021). The 10-fold cross-validation approach gauges the utility of the AMD model in real-world applications. It divides the dataset into ten subsets, using one subset for validation and the others for training in each iteration. This process is repeated ten times, with each data point used only once for validation. The final result is reported as the average of the ten validations.

The performance of the image-based model is enhanced by considering certain features, namely sex, rash site, and age, as detailed in Section 3.3.1. The feature rates are presented in Table 3 (sex and rash site) and Table 4 (age). As depicted in Table 3, males and females exhibit melanoma with medium and low probability, respectively. The table further illustrates that the head, neck, oral, and genital regions are associated with a high probability of melanoma, the upper extremity demonstrates a medium probability, and the lower extremity, palms, soles, and torso regions are linked to a low probability of melanoma. Additionally, the last row of the table indicates that our proposed mechanism has utilized all 33,125 images to derive a metadata-based model (encompassing sex and rash site ranges). It also reveals that 584 images manifest melanoma, with a ToPR (percentage of melanoma-suffering images) of 1.76.

Table 4 illustrates the impact of age on the likelihood of developing melanoma. It indicates that patients aged 0–10, 10–55, 55–60, 65–75, and 75–90 exhibit melanoma with very low, low, medium, high, and very high probability, respectively. The numerical statistics highlight an escalating probability of developing melanoma with increasing patient age.

To evaluate the performance of AMD, simulations for all steps were conducted using MATLAB R2018a on a computer running the Windows 10 operating system, equipped with an Intel (R) Core (TM) i7-3520 M CPU @ 2.90 GHz and 8 GB RAM.

4.1. Results of image-based model

This section examines cross-validation error, true positive, true negative, false positive, false negative, precision, sensitivity, accuracy, F-value, and the computational time indicators to assess the performance of classifiers utilized in our proposed mechanism (DT, K-NN, and SVM). It should be noted that the SVM parameters used in the experiments are the defaults of the MATLAB R2018a SVM function (fitcsvm) (Mathworks, 2022c):

- Kernel Function: Linear
- Box Constraint: 1
- Kernel Scale: auto
- Standardize: true

Table 3
Sex and rash site rates in the dataset (ISIC 2020).

Feature	Domain	Code	#Image	#Positive	Positive Rate(%)	IF
Sex	female	0	15,981	220	1.37	Low
	male	1	17,079	364	2.13	Medium
	unknown	2	65	0	–	
Rash site	head/neck	0	1854	74	3.99	High
	lower extremity	1	8417	124	1.47	Low
	oral/genital	2	124	4	3.22	High
	palms/soles	3	375	5	1.33	Low
	torso	4	16,845	257	1.52	Low
	upper extremity	5	4983	111	2.22	Medium
	Unknown	6	527	9	1.7	low
			Total	33,125	584	**ToPR** = 1.76

Table 4
Age rates in the dataset (ISIC 2020).

Age	Positive Frequency	Total Frequency	Positive Rate %	IF
−1	0	68	0	Very Low
0	0	2	0	Very Low
10	0	17	0	Very Low
15	2	132	1.52	Low
20	6	655	0.92	Low
25	16	1544	1.04	Low
30	24	2358	1.02	Low
35	25	2850	0.88	Low
40	24	3576	0.67	Low
45	54	4465	1.21	Low
50	53	4270	1.24	Low
55	64	3824	1.67	Low
60	65	3240	2.01	Medium
65	70	2527	2.77	High
70	58	1968	2.95	High
75	62	981	6.32	Very High
80	36	419	8.59	Very High
85	9	149	6.04	Very High
90	16	80	20.00	Very High

The cross-validation error signifies the regression model's error (mean squared error) (Alqudah et al., 2021). Specifically, the error of each non-training layer is computed based on the k-layer cross-validation model and the training layer. As shown in the 2nd column of Table 5, the cross-validation error (k-Fold Loss (k = 10)) is reduced by 55.05 % and 97.26 % when using DT compared to the K-NN and SVM classifiers, respectively. This indicates that DT performs better than other classifiers in error-sensitive applications such as melanoma detection in dermoscopic images.

True Positive (TP) represents an output where AMD correctly predicts the positive class (melanoma-suffering skins) (Turner et al., 2021). Similarly, True Negative (TN) refers to an outcome where the model correctly predicts the negative class (healthy skin) (Ningrum et al., 2021). False Positive (FP) is an output where AMD does not correctly predict the positive class (Thompson et al., 2021). Finally, False Negative (FN) refers to an outcome where the model does not correctly predict the negative class (Dieng et al., 2021). As illustrated in the 3rd-6th columns of Table 5, DT exhibits 1.26 and 4.2 times better performance than K-NN and SVM classifiers in true positive evaluation, respectively. The results also indicate that DT is 1.08 and 3.55 times better than others in detecting negative samples. True/false positive outcomes demonstrate the superiority of DT in automated melanoma detection.

Accuracy (detection rate) is a fundamental indicator in evaluating the performance of automated skin disease detection mechanisms, representing the number of images that match the training data correctly (MEJÀRE et al., 1985). The accuracy (A) is calculated as (9) (MEJÀRE et al., 1985):

$$A = \frac{TP + TN}{P + N} \tag{9}$$

where P and N indicate the number of melanoma-suffering and healthy images, respectively. The 7th column of Table 5 demonstrates that the

Table 5
Comparison of classifiers used in the image-based model.

Classifier	cross-validation error	true positive	true negative	false positive	false negative	accuracy	precision	sensitivity	F-value	Time (s)
DT	0.008	63	26	64	21	0.511	0.49	0.75	0.59	0.49
K-NN	0.0187	50	31	59	34	0.46	0.458	0.595	0.51	6.12
SVM	0.2927	15	72	18	69	0.5	0.45	0.178	0.25	168.9

mechanism's accuracy, in the case of using the DT classifier, is 1.11 and 1.02 times higher than the K-NN and SVM ones, respectively. It can be argued that the DT, SVM, and K-NN classifiers provide the most accurate performance in automated melanoma detection in descending order.

Sensitivity measures the completeness of classification algorithms, indicating the percentage of positive samples (melanoma-suffering images) labelled correctly (McDonald, 2019). Sensitivity (S) is defined as (10) (McDonald, 2019):

$$S = \frac{TP}{P} \tag{10}$$

where P is the number of melanoma-suffering images. The 8th column of Table 5 shows that DT performs better than other classifiers by maximizing sensitivity. It indicates that the sensitivity of our mechanism, in the case of using DT, is 1.26 and 4.21 times higher than K-NN and SVM classifiers, respectively. As a result, DT is more sensitive than others in detecting true positive samples.

Precision is a standard criterion for assessing the correctness of classification algorithms, determining what percentage of the samples (dermoscopic images) labelled as positive are melanoma-suffering skins (MEJÀRE et al., 1985). Precision (Pr) is calculated as (11) (MEJÀRE et al., 1985):

$$Pr = \frac{TP}{TP + FP} \tag{11}$$

The 9th column of Table 5 demonstrates that DT labels melanoma-suffering samples with 49 % precision. In more detail, the numerical results illustrate that the mechanism's precision, in the case of using DT, is 1.06 and 1.08 times higher than K-NN and SVM, respectively. Thus, DT is a suitable algorithm for sample classification in critical applications such as melanoma detection.

The fundamental factor in evaluating the performance of proposed models to classify dermoscopic images is the harmonic mean of sensitivity and accuracy called the F-value (Fushiki, 2011). It is defined as (12) (Fushiki, 2011):

$$F - value = \frac{2 \times Pr \times S}{Pr + S} \tag{12}$$

As shown in the 10th column of Table 5, the F-value in the case of using DT is 1.15 and 3.93 times better than the K-NN and SVM classifiers, respectively. Accordingly, it can be argued that DT classifies dermoscopic images better than others.

Finally, the 11th column of Table 5 presents the time spent, a crucial metric measured in the experimental results. It indicates that the computational time is 12.48 and 344.69 times more efficient when using DT compared to K-NN and SVM classifiers, respectively. In conclusion, the substantial efficiency gain observed in the execution time for the DT classifier underscores its computational superiority over the K-NN and SVM classifiers. This efficiency is particularly noteworthy in real-time applications or scenarios where rapid processing is imperative. The considerable time advantage exhibited by DT contributes to the overall appeal of the AMD model, making it not only a robust performer in terms of accuracy and sensitivity but also a computationally efficient solution for automated melanoma detection on dermoscopic images.

In this stage, the precise values for TP, FN, FP, and TN obtained from the experimental results are inserted into the confusion matrix (Božić et al., 2023), offering a more detailed interpretation. This data offers valuable insights into the AMD model's effectiveness in categorizing dermoscopic images. Fig. 7 (a), (b), and (c) depict the confusion matrix for DT, K-NN, and SVM, respectively.

4.2. Results of metadata-based model

In this section, the impact coefficients of the decision criteria and the main threshold are tuned for high sensitivity and accuracy, including W_0, W_1, W_2, W_3 and $Threshold_{Main}$ for the image-based model (DT classifier), sex, age, rash site, and the pre-determined threshold, respectively. Four scenarios are defined for tuning the impact coefficients of the decision criteria, as shown in Table 6. The first scenario focuses on *meta*-features, and the image-based model is partially considered. Scenarios second to four gradually reduce the impact coefficients of *meta*-features and focus more on the image-based model. Numerical results demonstrate that accuracy and F-value are improved 1.18 and 1.15 times on average when using the first scenario compared to others by focusing on *meta*-features. Thus, the first scenario with $W_0 = 0.1$, $W_1 = 0.2$, $W_2 = 0.35$, and $W_3 = 0.35$ can be considered the best one.

It should be noted that we set $Threshold_{Main} = 0.43$ based on experimental analyses of the dataset. As shown in Fig. 8, the intersection of four diagrams of precision, sensitivity, accuracy, and F-value is considered as $Threshold_{Main}$ for scenarios one to three (Fig. 8 (a–c)) to achieve a balance between performance criteria. Since we highlight the first scenario, the intersection of diagrams in Fig. 8 (a) is considered the selected $Threshold_{Main}$. It is worth mentioning that the value of these criteria is independent of $Threshold_{Main}$ in the fourth scenario (Fig. 8 (d)); their impact coefficients are considered zero. Thus, we can consider any value for $Threshold_{Main}$ in this scenario, it is set to the mean value (0.5).

Finally, Fig. 9 illustrates the precision-recall curve of the AMD model for the best scenario. The precision-recall curve serves as a valuable tool for assessing the classification model's performance, including DT. It visualizes the trade-off between precision and sensitivity (recall) at various DT thresholds, showcasing how well the proposed model can identify positive instances while keeping false positives to a minimum (Miao and Zhu, 2022). A high-precision model exercises caution in predicting positives but maintains accuracy when it does, while a high-recall (sensitivity) model captures a substantial portion of actual positives but may generate more false positives. The ideal situation aims for both high precision and high recall, yet a trade-off often exists between these two metrics.

For the AMD model, the precision-recall curve aids in comprehending the model's performance across diverse decision boundaries. It assists in selecting a suitable threshold aligned with the specific requirements of the application. As shown in Fig. 9, the optimal point on the curve is specified as (X = 0.6548, Y = 0.7143) for our melanoma detection mechanism. This optimal threshold allows for the effective identification of melanoma cases with a high level of accuracy (precision) while ensuring that a substantial proportion of actual positive cases is captured (recall). Therefore, by pinpointing this optimal operating point on the precision-recall curve, the AMD model can be fine-tuned to meet the desired performance criteria for melanoma detection.

4.3. Total results

In this section, the total implementation results are presented to prove the efficiency of AMD compared to recent state-of-the-art melanoma detection mechanisms on dermoscopic images based on the ISIC

		Predicted Condition			
	Total Population = 174	Positive (PP) =127	Negative (PN) = 47		
Actual Condition	Positive (P)= 84	**TP= 63**	**FN= 21**	True Positive Rate (TPR), Recall, **Sensitivity** (SEN), Probability of Detection, Hit Rate, Power $= \frac{TP}{P} = 0.75$	False Negative Rate (FNR), Miss Rate $= \frac{FN}{P} = 0.25$
	Negative (N) = 90	**FP= 64**	**TN= 26**	False positive rate (FPR), probability of false alarm, fall-out $= \frac{FP}{N} = 0.72$	True Negative Rate (TNR), Specificity (SPC), Selectivity $= \frac{TN}{N} = 0.28$
		Positive Predictive Value (PPV), **Precision** $= \frac{TP}{PP} = 0.49$	False Omission Rate (FOR) $= \frac{FN}{PN} = 0.44$	F1-score, **F-value** $= \frac{2 \times PPV \times TPR}{PPV + TPR} = 0.59$	
		False Discovery Rate (FDR) $= \frac{FP}{PP} = 0.50$	Negative predictive value (NPV) $= \frac{TN}{PN} = 0.55$	**Accuracy** (ACC) $= \frac{TP+TN}{P+N} = 0.511$	

(a)

Fig. 7. Confusion matrix: (a) DT, (b) K-NN, and (c) SVM.

2020 dataset. The first approach has been trained on the VGG19 deep learning architecture to analyze the dataset called "VGG19" (Cassidy et al., 2022). The second one is a deep CNN-based architecture for melanoma detection, which is called "InceptionV3" (Szegedy et al., 2015). The third mechanism has provided another balanced CNN-based model for melanoma detection on the ISIC dataset, called "ResNet152" (Cassidy et al., 2022). The critical performance factors of automated melanoma detection are analyzed for accurate evaluation, including precision, sensitivity, accuracy, and F-value.

As mentioned in Section 4.1, precision is a standard criterion to determine the percentage of melanoma-suffering dermoscopic images labelled as positive. The second column of Table 7 illustrates that AMD labels melanoma-suffering images with 71 % precision. The numerical results also demonstrate that the precision of our proposed mechanism is 3.55, 3.38, and 3.38 times better than VGG19, InceptionV3, and ResNet152, respectively. Thus, AMD can be introduced as a unique mechanism to improve identification performance in critical applications such as melanoma detection on dermoscopic images.

Sensitivity is a completeness indicator to demonstrate the percentage of melanoma-suffering images labelled correctly. The third column of Table 7 shows that our presented mechanism is 1.58 times more sensitive than VGG19 in melanoma detection. However, in the case of sensitivity, the InceptionV3 and ResNet152 approaches are 1.44 and 1.32 times better than AMD. Therefore, InceptionV3 is more sensitive than other mechanisms in detecting true positive dermoscopic images using the advantages of CNN.

Accuracy counts the number of test images matching the training ones. The fourth column of Table 7 illustrates that the accuracy of AMD is 1.25, 2.33, and 2.18 times better than VGG19, InceptionV3, and ResNet152, respectively. The results show that our proposed mechanism detects melanoma-suffering images more accurately than CNN-based ones.

Finally, the fifth column of Table 7 shows that AMD's F-value (the harmonic mean of sensitivity and accuracy) is 2.61, 2, and 2.06 times higher than VGG19, InceptionV3, and ResNet152 approaches, respectively. Although the sensitivity of InceptionV3 and ResNet152 architecture is better than our presented mechanism, the F-value indicates that AMD generally detects melanoma on dermoscopic images superior to others.

5. Limitation and discussion

In this section, we provide a thorough exploration of the limitations and discussion of AMD.

5.1. Limitation

While our proposed model shows promising results in automated melanoma detection, it is essential to acknowledge its limitations. These items are categorized as follows:

- *Dataset Specificity*: The model's performance heavily relies on the quality and representativeness of the training dataset. If the dataset is biased or lacks diversity, the model may not generalize well to different populations, ethnicities, or skin types.
- *Dependency on Dermoscopic Imaging*: AMD's effectiveness is contingent on the availability of high-quality dermoscopic images. In real-world scenarios where such images might be challenging to obtain, the model's performance could be compromised.
- *Sensitivity to Pre-processing Parameters*: The pre-processing steps, including artifact removal and image standardization, involve parameter tuning. Sensitivity to these parameters might affect the model's robustness across different datasets and conditions.

		Predicted Condition			
	Total Population = 174	Positive (PP) = 109	Negative (PN) = 65		
Actual Condition	Positive (P)= 84	**TP= 50**	**FN= 34**	True Positive Rate (TPR), Recall, **Sensitivity** (SEN), Probability of Detection, Hit Rate, Power $= \frac{TP}{P} = 0.595$	False Negative Rate (FNR), Miss Rate $= \frac{FN}{P} = 0.405$
	Negative (N) = 90	**FP= 59**	**TN= 31**	False positive rate (FPR), probability of false alarm, fall-out $= \frac{FP}{N} = 0.65$	True Negative Rate (TNR), Specificity (SPC), Selectivity $= \frac{TN}{N} = 0.35$
		Positive Predictive Value (PPV), **Precision** $= \frac{TP}{PP} = 0.458$	False Omission Rate (FOR) $= \frac{FN}{PN} = 0.52$	F1-score, **F-value** $= \frac{2 \times PPV \times TPR}{PPV + TPR} = 0.51$	
		False Discovery Rate (FDR) $= \frac{FP}{PP} = 0.542$	Negative predictive value (NPV) $= \frac{TN}{PN} = 0.48$	**Accuracy** (ACC) $= \frac{TP+TN}{P+N} = 0.46$	

(b)

		Predicted Condition			
	Total Population = 174	Positive (PP) = 33	Negative (PN) = 141		
Actual Condition	Positive (P)= 84	**TP= 15**	**FN= 69**	True Positive Rate (TPR), Recall, **Sensitivity** (SEN), Probability of Detection, Hit Rate, Power $= \frac{TP}{P} = 0.178$	False Negative Rate (FNR), Miss Rate $= \frac{FN}{P} = 0.822$
	Negative (N) = 90	**FP= 18**	**TN= 72**	False positive rate (FPR), probability of false alarm, fall-out $= \frac{FP}{N} = 0.2$	True Negative Rate (TNR), Specificity (SPC), Selectivity $= \frac{TN}{N} = 0.8$
		Positive Predictive Value (PPV), **Precision** $= \frac{TP}{PP} = 0.45$	False Omission Rate (FOR) $= \frac{FN}{PN} = 0.49$	F1-score, **F-value** $= \frac{2 \times PPV \times TPR}{PPV + TPR} = 0.25$	
		False Discovery Rate (FDR) $= \frac{FP}{PP} = 0.55$	Negative predictive value (NPV) $= \frac{TN}{PN} = 0.51$	**Accuracy** (ACC) $= \frac{TP+TN}{P+N} = 0.5$	

(c)

Fig. 7. (*continued*).

5.2. Discussion

The AMD model introduces advancements in melanoma detection, but several aspects merit discussion for future improvements and research directions, as follows:

- *Integration of Clinical Data*: Incorporating additional clinical data, such as patient history or genetic information, could enhance the

Table 6
Impact coefficients of the decision criteria.

Scenario	Coefficient of image-based model	Coefficient of *meta*-features			Results			Description
	W_0	W_1	W_2	W_3	Threshold_{Main}	Accuracy	F-value	
1	**0.1**	**0.2**	**0.35**	**0.35**	**0.43**	**0.70**	**0.68**	More focus on metadata
2	0.2	0.2	0.3	0.3	0.46	0.64	0.62	
3	0.7	0.1	0.1	0.1	0.81	0.63	0.56	
4	1	0	0	0	0.5	0.51	0.59	focus on the image-based model

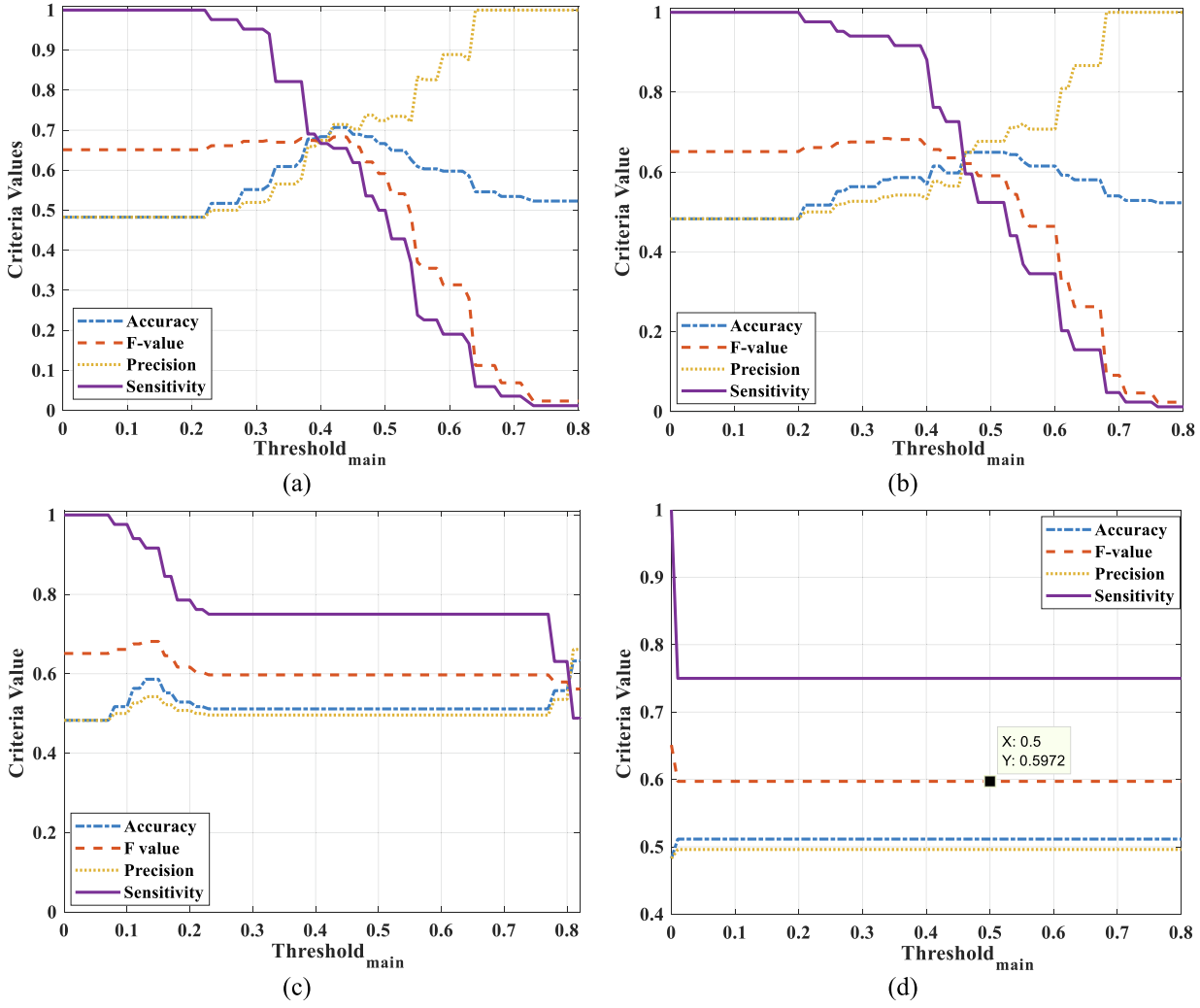

Fig. 8. *Threshold*$_{main}$ of scenarios: (a) First, (b) Second, (c) Third, and (d) Fourth ones.

model's predictive power. Collaborations with healthcare professionals may provide valuable insights.

- *Real-time Application*: Discussions should consider the model's potential application in real-time scenarios, such as telemedicine or mobile applications. Ensuring efficiency and speed without compromising accuracy is crucial for practical deployment.
- *Ethical Considerations*: Discussions should extend to ethical implications, including data privacy, bias in model predictions, and potential consequences of false positives or negatives. Balancing these considerations is pivotal for responsible AI deployment in healthcare.
- *User-Friendliness*: For widespread adoption, considerations about user-friendliness and integration into existing healthcare systems should be addressed.

In conclusion, while the AMD mechanism presents a significant stride in melanoma detection, continuous refinement, validation on diverse datasets, and addressing ethical considerations are pivotal for its successful integration into clinical practice.

6. Conclusion and future works

This paper introduces a novel mechanism for automated melanoma detection in dermoscopic images. The proposed approach involves multiple steps to enhance the processing and reliability of melanoma detection. In the initial phase, patient information and hair artifacts are removed from raw images, and the remaining pixels are standardized for improved resolution. The second step employs techniques such as Radon transform, Top-hat filter, and features like DWT and DCT to enhance AMD's reliability, remove unnecessary data, and increase the detection

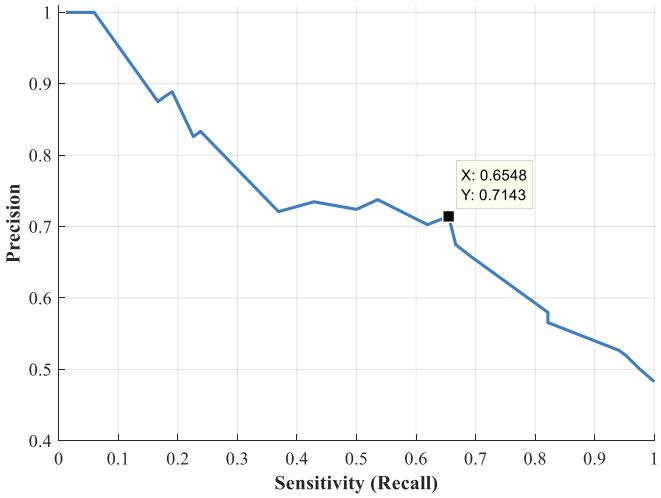

Fig. 9. Precision-recall curve.

Table 7
Comparison of melanoma detection approaches.

Approaches	Precision	Sensitivity	Accuracy	F-value
AMD	0.71	0.65	0.70	0.68
VGG19 (Cassidy et al., 2022)	0.20	0.41	0.56	0.26
InseptionV3 (Szegedy et al., 2015)	0.21	0.94	0.30	0.34
ResNet152 (Cassidy et al., 2022)	0.21	0.86	0.32	0.33

rate. Further, DCT coefficients are converted into a 1D vector using Zigzag, and the feature count is reduced with LSDA. In the third step, processed images are categorized into training and test data. Various image-based models are created using the training data, and the best model is selected based on evaluation with test data. Lastly, the metadata-based model refines the performance of the image-based model using sex, rash site, and age as key features. Simulation results for the image-based model indicate that DT outperforms other classifiers in accurately and sensitively classifying dermoscopic images, showing improvement in F-Value. Besides, DT demonstrates superior performance compared to K-NN and SVM by minimizing cross-validation errors in automated melanoma detection. Finally, comparison results highlight that the hybrid AMD model, integrating image and metadata-based approaches, outperforms other state-of-the-art methods in melanoma detection in dermoscopic images, improving the harmonic mean of sensitivity and accuracy.

The proposed AMD mechanism lays a foundation for enhanced automated melanoma detection; however, several avenues for future research and improvement can be explored:

- *Dataset Diversity*: Expanding the dataset to include a more diverse range of skin types, ethnicities, and geographical locations would contribute to a more robust and generalizable model. This would ensure the effectiveness of the AMD mechanism across various populations.
- *Real-world Clinical Validation*: Conducting extensive clinical trials and validations involving dermatologists and healthcare practitioners is essential to assess the real-world applicability and accuracy of the AMD model. This step is crucial before considering the integration of the mechanism into clinical settings.
- *Ethical Considerations*: Addressing ethical concerns related to patient privacy, informed consent, and data security is imperative. Future work should focus on developing and implementing ethical guidelines to govern the deployment of AMD in medical settings.
- *Online Learning and Adaptation*: Implementing mechanisms for continuous learning and adaptation is essential to keep the model updated with emerging melanoma characteristics and evolving medical knowledge. This ensures that the AMD model remains relevant and effective over time.
- *Integration with Clinical Workflows*: Streamlining the integration of the AMD mechanism into existing clinical workflows is vital for its practical adoption. Future work should explore ways to seamlessly incorporate AMD into diagnostic processes and electronic health record systems.
- *Collaboration with Dermatology Experts*: Collaboration with dermatologists and domain experts is critical for refining the AMD mechanism. Involving dermatologists in the model development process and incorporating their feedback will enhance the model's accuracy and clinical relevance.
- *Mobile Application Development*: Designing a user-friendly mobile application for dermatologists and healthcare practitioners could facilitate easy access to the AMD model. Such an application could provide quick and efficient melanoma risk assessments during routine clinical examinations.

By addressing these aspects in future research, the AMD mechanism can evolve into a more potent tool for melanoma detection, offering improved accuracy, ethical adherence, and seamless integration into clinical practice.

Data availability statement

Data will be available from corresponding authors upon reasonable request for academic purposes.

Declaration of competing interest

The authors declare that they have no known competing financial interests or personal relationships that could have appeared to influence the work reported in this paper.

References

Abbas, Q., Ramzan, F., Ghani, M.U., 2021. Acral melanoma detection using dermoscopic images and convolutional neural networks. Vis. Comput. Ind. Biomed. Art 4, 25. https://doi.org/10.1186/s42492-021-00091-z.

Abbes, W., Sellami, D., Marc-Zwecker, S., Zanni-Merk, C., 2021. Fuzzy decision ontology for melanoma diagnosis using KNN classifier. Multimed. Tools Appl. 80, 25517–25538. https://doi.org/10.1007/s11042-021-10858-4.

Acharya, U.R., Mookiah, M.R.K., Koh, J.E.W., Tan, J.H., Bhandary, S.V., Rao, A.K., Hagiwara, Y., Chua, C.K., Laude, A., 2017. Automated diabetic macular edema (DME) grading system using DWT, DCT Features and maculopathy index. Comput. Biol. Med. 84, 59–68. https://doi.org/10.1016/j.compbiomed.2017.03.016.

Adegun, A., Viriri, S., 2021. Deep learning techniques for skin lesion analysis and melanoma cancer detection: a survey of state-of-the-art. Artif. Intell. Rev. 54, 811–841. https://doi.org/10.1007/s10462-020-09865-y.

Alheejawi, S., Berendt, R., Jha, N., Maity, S.P., Mandal, M., 2021. Automated proliferation index calculation for skin melanoma biopsy images using machine learning. Comput. Med. Imaging Graph. 89, 101893 https://doi.org/10.1016/j.compmedimag.2021.101893.

Alqudah, A.M., Qazan, S., Masad, I.S., 2021. Artificial intelligence framework for efficient detection and classification of pneumonia using chest radiography images. J. Med. Biol. Eng. https://doi.org/10.1007/s40846-021-00631-1.

Bai, J., Li, Y., Li, J., Yang, X., Jiang, Y., Xia, S.-T., 2022. Multinomial random forest. Pattern Recogn. 122, 108331 https://doi.org/10.1016/j.patcog.2021.108331.

Benyahia, S., Meftah, B., Lézoray, O., 2022. Multi-features extraction based on deep learning for skin lesion classification. Tissue Cell 74, 101701. https://doi.org/10.1016/j.tice.2021.101701.

Božić, D., Runje, B., Lisjak, D., Kolar, D., 2023. Metrics related to confusion matrix as tools for conformity assessment decisions. Appl. Sci. 13, 8187. https://doi.org/10.3390/app13148187.

Cassidy, B., Kendrick, C., Brodzicki, A., Jaworek-Korjakowska, J., Yap, M.H., 2022. Analysis of the ISIC image datasets: usage, benchmarks and recommendations. Med. Image Anal. 75, 102305 https://doi.org/10.1016/j.media.2021.102305.

Chakkaravarthy, A.P., Chandrasekar, A., 2020. Anatomical region segmentation method from dermoscopic images of pigmented skin lesions. Int. J. Imaging Syst. Technol. 30, 636–652. https://doi.org/10.1002/ima.22404.

Daghrir, J., Tlig, L., Bouchouicha, M., Sayadi, M., 2020. Melanoma skin cancer detection using deep learning and classical machine learning techniques: a hybrid approach. In: 2020 5th International Conference on Advanced Technologies for Signal and Image Processing (ATSIP). IEEE, pp. 1–5. https://doi.org/10.1109/ATSIP49331.2020.9231544.

Dieng, M., Lord, S.J., Nieweg, O.E., Saw, R.P.M., Einstein, A.J., Nijhuis, A.A.G., Turner, R.M., Thompson, J.F., Morton, R.L., 2021. Reply to: CT and PET/CT surveillance in stage iiia-d melanoma results in more false-positive than true-positive findings and should not be routinely recommended, by nicholas taylor et al. Ann. Surg. Oncol. 28, 819–820. <https://doi.org/10.1245/s10434-021-09821-2>.

Doms, V., Gordienko, Y., Kochura, Y., Rokovyi, O., Alienin, O., Stirenko, S., 2021. Deep Learning for Melanoma Detection with Testing Time Data Augmentation. pp. 131–140. <https://doi.org/10.1007/978-3-030-80475-6_13>.

Efimenko, M., Ignatev, A., Koshechkin, K., 2020. Review of medical image recognition technologies to detect melanomas using neural networks. BMC Bioinform. 21, 270. https://doi.org/10.1186/s12859-020-03615-1.

Eliwa, E.H.I., El Koshiry, A.M., Abd El-Hafeez, T., Farghaly, H.M., 2023. Utilizing convolutional neural networks to classify monkeypox skin lesions. Sci. Rep. 13, 14495. https://doi.org/10.1038/s41598-023-41545-z.

Eman, M., Mahmoud, T.M., Ibrahim, M.M., Abd El-Hafeez, T., 2023. Innovative hybrid approach for masked face recognition using pretrained mask detection and segmentation, robust PCA, and KNN classifier. Sensors 23, 6727. https://doi.org/10.3390/s23156727.

Fushiki, T., 2011. Estimation of prediction error by using K-fold cross-validation. Stat. Comput. 21, 137–146. https://doi.org/10.1007/s11222-009-9153-8.

Gajera, H.K., Zaveri, M.A., Nayak, D.R., 2021. Improving the performance of melanoma detection in dermoscopy images using deep CNN features. pp. 349–354. <https://doi.org/10.1007/978-3-030-77211-6_39>.

Gálvez, A., Iglesias, A., Fister, I., Fister, I., Otero, C., Díaz, J.A., 2021. NURBS functional network approach for automatic image segmentation of macroscopic medical images in melanoma detection. J. Comput. Sci. 56, 101481 https://doi.org/10.1016/j.jocs.2021.101481.

Gareau, D.S., Browning, J., Correa Da Rosa, J., Suarez-Farinas, M., Lish, S., Zong, A.M., Firester, B., Vrattos, C., Renert-Yuval, Y., Gamboa, M., Vallone, M.G., Barragán-Estudillo, Z.F., Tamez-Peña, A.L., Montoya, J., Jesús-Silva, M.A., Carrera, C., Malvehy, J., Puig, S., Marghoob, A., Carucci, J.A., Krueger, J.G., 2020. Deep learning-level melanoma detection by interpretable machine learning and imaging biomarker cues. J. Biomed. Opt. 25 https://doi.org/10.1117/1.JBO.25.11.112906.

Hou, P., Bao, S., Fan, D., Yan, C., Su, J., Qu, J., Zhou, M., 2021. Machine learning-based integrative analysis of methylome and transcriptome identifies novel prognostic DNA methylation signature in uveal melanoma. Brief. Bioinform. 22 https://doi.org/10.1093/bib/bbaa371.

Huang, M., Zhang, Y., Ou, X., Wang, C., Wang, X., Qin, B., Zhang, Q., Yu, J., Zhang, J., Yu, J., 2021. m5C-related signatures for predicting prognosis in cutaneous melanoma with machine learning. J. Oncol. 2021, 1–14. https://doi.org/10.1155/2021/6173206.

Jing, E., Zhang, H., Li, Z., Liu, Y., Ji, Z., Ganchev, I., 2021. ECG heartbeat classification based on an improved ResNet-18 model. Comput. Math. Methods Med. 2021, 1–13. https://doi.org/10.1155/2021/6649970.

Kaminsky, A.L., Wang, Y., Pant, K., 2021. An efficient batch K-fold cross-validation voronoi adaptive sampling technique for global surrogate modeling. J. Mech. Des. 143 https://doi.org/10.1115/1.4047155.

Kassem, M.A., Hosny, K.M., Damaševičius, R., Eltoukhy, M.M., 2021. Machine learning and deep learning methods for skin lesion classification and diagnosis: a systematic review. Diagnostics 11, 1390. https://doi.org/10.3390/diagnostics11081390.

Khan, M.S., Alam, K.N., Dhruba, A.R., Zunair, H., Mohammed, N., 2022. Knowledge distillation approach towards melanoma detection. Comput. Biol. Med. 146, 105581 https://doi.org/10.1016/j.compbiomed.2022.105581.

Kumar Tiwari, A., Kumar Mishra, M., Ranjan Panda, A., Panda, B., 2021. Hosmi-lbp-based feature extraction for melanoma detection using hybrid deep learning models. J. Mech. Med. Biol. 21, 2150029. <https://doi.org/10.1142/S0219519421500299>.

Kurdi, H., Alkubeyyer, A., Alabdullatif, R., Althnian, A., 2022. Classification of Mammogram Masses Using GLCM on LBP and Non-overlapping Blocks of Varying Sizes. pp. 253–266. <https://doi.org/10.1007/978-981-16-5348-3_20>.

Lagani, G., Falchi, F., Gennaro, C., Amato, G., 2022. Comparing the performance of Hebbian against backpropagation learning using convolutional neural networks. Neural Comput. Appl. 34, 6503–6519. https://doi.org/10.1007/s00521-021-06701-4.

Lu, H., Ma, X., 2020. Hybrid decision tree-based machine learning models for short-term water quality prediction. Chemosphere 249, 126169. https://doi.org/10.1016/j.chemosphere.2020.126169.

Lu, T., Yu, F., Xue, C., Han, B., 2021. Identification, classification, and quantification of three physical mechanisms in oil-in-water emulsions using AlexNet with transfer learning. J. Food Eng. 288, 110220 https://doi.org/10.1016/j.jfoodeng.2020.110220.

Magalhaes, C., Tavares, J.M.R.S., Mendes, J., Vardasca, R., 2021. Comparison of machine learning strategies for infrared thermography of skin cancer. Biomed. Signal Process. Control 69, 102872. https://doi.org/10.1016/j.bspc.2021.102872.

Mathworks [WWW Document], 2022. URL https://www.mathworks.com/ (Accessed 2.14.22).

McDonald, G., 2019. A framework for technology-assisted sensitivity review. ACM SIGIR Forum 53, 42–43. https://doi.org/10.1145/3458537.3458544.

Mejàre, I., Gröndahl, H.-G., Carlstedt, K., Grever, A.-C., Ottosson, E., 1985. Accuracy at radiography and probing for the diagnosis of proximal caries. Eur. J. Oral Sci. 93, 178–184. https://doi.org/10.1111/j.1600-0722.1985.tb01328.x.

Miao, J., Zhu, W., 2022. Precision–recall curve (PRC) classification trees. Evol. Intell. 15, 1545–1569. https://doi.org/10.1007/s12065-021-00565-2.

Mirikharaji, Z., Abhishek, K., Bissoto, A., Barata, C., Avila, S., Valle, E., Celebi, M.E., Hamarneh, G., 2023. A survey on deep learning for skin lesion segmentation. Med. Image Anal. 88, 102863 https://doi.org/10.1016/j.media.2023.102863.

Mohd-Isa, W.-N., Joseph, J., Hashim, N., Salih, N., 2021. Enhancement of digitized X-ray films using Contrast-Limited Adaptive Histogram Equalization (CLAHE). F1000Research 10, 1051. https://doi.org/10.12688/f1000research.73236.1.

Murugan, A., Nair, S.A.H., Kumar, K.P.S., 2019. Abbes. J. Med. Syst. 43, 269. https://doi.org/10.1007/s10916-019-1400-8.

Nawaz, M., Mehmood, Z., Nazir, T., Naqvi, R.A., Rehman, A., Iqbal, M., Saba, T., 2022. Skin cancer detection from dermoscopic images using deep learning and fuzzy k -means clustering. Microsc. Res. Tech. 85, 339–351. https://doi.org/10.1002/jemt.23908.

Ningrum, D.N.A., Yuan, S.-P., Kung, W.-M., Wu, C.-C., Tzeng, I.-S., Huang, C.-Y., Li, J.-Y.-C., Wang, Y.-C., 2021. Deep learning classifier with patient's metadata of dermoscopic images in malignant melanoma detection. J. Multidiscip. Healthc. 14, 877–885. https://doi.org/10.2147/JMDH.S306284.

Patil, R., Bellary, S., 2020. Machine learning approach in melanoma cancer stage detection. J. King Saud Univ. - Comput. Inf. Sci. https://doi.org/10.1016/j.jksuci.2020.09.002.

Pereira, P.M.M., Thomaz, L.A., Tavora, L.M.N., Assuncao, P.A.A., Fonseca-Pinto, R.M., Paiva, R.P., de Faria, S.M.M., 2022. Melanoma classification using light-Fields with morlet scattering transform and CNN: Surface depth as a valuable tool to increase detection rate. Med. Image Anal. 75, 102254 https://doi.org/10.1016/j.media.2021.102254.

Ramos-Soto, O., Rodríguez-Esparza, E., Balderas-Mata, S.E., Oliva, D., Hassanien, A.E., Meleppat, R.K., Zawadzki, R.J., 2021. An efficient retinal blood vessel segmentation in eye fundus images by using optimized top-hat and homomorphic filtering. Comput. Methods Programs Biomed. 201, 105949 https://doi.org/10.1016/j.cmpb.2021.105949.

Raza, R., Zulfiqar, F., Tariq, S., Anwar, G.B., Sargano, A.B., Habib, Z., 2021. Melanoma classification from dermoscopy images using ensemble of convolutional neural networks. Mathematics 10, 26. https://doi.org/10.3390/math10010026.

Saabia, A.A.-B., El-Hafeez, T., Zaki, A.M., 2019. Face Recognition Based on Grey Wolf Optimization for Feature Selection. pp. 273–283. https://doi.org/10.1007/978-3-319-99010-1_25.

Scott, S.B., Sliwinski, M.J., Zawadzki, M., Stawski, R.S., Kim, J., Marcusson-Clavertz, D., Lanza, S.T., Conroy, D.E., Buxton, O., Almeida, D.M., Smyth, J.M., 2020. A coordinated analysis of variance in affect in daily life. Assessment 27, 1683–1698. https://doi.org/10.1177/1073191118799460.

Shajahan, M., Aris, S.A.M., Usman, S., Noor, N.M., 2021. IRPMID: Medical XRAY Image Impulse Noise Removal using Partition Aided Median, Interpolation and DWT. In: 2021 IEEE International Conference on Signal and Image Processing Applications (ICSIPA). IEEE, pp. 105–110. https://doi.org/10.1109/ICSIPA52582.2021.9576773.

Szegedy, C., Liu, W., Jia, Y., Sermanet, P., Reed, S., Anguelov, D., Erhan, D., Vanhoucke, V., Rabinovich, A., 2015. Going deeper with convolutions, in: In Proceedings of the IEEE Conference on Computer Vision and Pattern Recognition. pp. 1–9.

Thiyaneswaran, B., Anguraj, K., Kumarganesh, S., Thangaraj, K., 2021. Early detection of melanoma images using gray level co-occurrence matrix features and machine learning techniques for effective clinical diagnosis. Int. J. Imaging Syst. Technol. 31, 682–694. https://doi.org/10.1002/ima.22514.

Thompson, J.F., Haydu, L.E., Uren, R.F., Andtbacka, R.H., Zager, J.S., Beitsch, P.D., Agnese, D.M., Mozzillo, N., Testori, A., Bowles, T.L., Hoekstra, H.J., Kelley, M.C., Sussman, J., Schneebaum, S., Smithers, B.M., McKinnon, G., Hsueh, E., Jacobs, L., Schultz, E., Reintgen, D., Kane, J.M., Friedman, E.B., Wang, H., Van Kreuningen, L., Schiller, V., Elashoff, D.A., Elashoff, R., Cochran, A.J., Stern, S., Faries, M.B., 2021. Preoperative ultrasound assessment of regional lymph nodes in melanoma patients does not provide reliable nodal staging. Ann. Surg. 273, 814–820. https://doi.org/10.1097/SLA.0000000000003405.

Tumpa, P.P., Kabir, M.A., 2021. An artificial neural network based detection and classification of melanoma skin cancer using hybrid texture features. Sensors Int. 2, 100128 https://doi.org/10.1016/j.sintl.2021.100128.

Turner, R.M., Dieng, M., Khanna, N., Nguyen, M., Zeng, J., Nijhuis, A.A.G., Nieweg, O.E., Einstein, A.J., Emmett, L., Lord, S.J., Menzies, A.M., Thompson, J.F., Saw, R.P.M., Morton, R.L., 2021. Performance of long-term CT and PET/CT surveillance for detection of distant recurrence in patients with resected stage IIIA–D melanoma. Ann. Surg. Oncol. 28, 4561–4569. https://doi.org/10.1245/s10434-020-09270-3.

Wang, Y., Cai, J., Louie, D.C., Wang, Z.J., Lee, T.K., 2021. Incorporating clinical knowledge with constrained classifier chain into a multimodal deep network for melanoma detection. Comput. Biol. Med. 137, 104812 https://doi.org/10.1016/j.compbiomed.2021.104812.

Wang, X., Chen, X., 2021. An image encryption algorithm based on dynamic row scrambling and Zigzag transformation. Chaos, Solitons & Fractals 147, 110962. https://doi.org/10.1016/j.chaos.2021.110962.

Wang, Y., Feng, Y., Zhang, L., Zhou, J.T., Liu, Y., Goh, R.S.M., Zhen, L., 2022. Adversarial multimodal fusion with attention mechanism for skin lesion classification using clinical and dermoscopic images. Med. Image Anal. 81, 102535 https://doi.org/10.1016/j.media.2022.102535.

Wang, Y., Wang, Y., Cai, J., Lee, T.K., Miao, C., Wang, Z.J., 2023. SSD-KD: a self-supervised diverse knowledge distillation method for lightweight skin lesion classification using dermoscopic images. Med. Image Anal. 84, 102693 https://doi.org/10.1016/j.media.2022.102693.

Wu, H., Xie, P., Zhang, H., Li, D., Cheng, M., 2020. Predict pneumonia with chest X-ray images based on convolutional deep neural learning networks. J. Intell. Fuzzy Syst. 39, 2893–2907. https://doi.org/10.3233/JIFS-191438.

Yao, H., Zhang, Y., Wei, Y., Tian, Y., 2020. Broad learning system with locality sensitive discriminant analysis for hyperspectral image classification. Math. Probl. Eng. 2020, 1–16. https://doi.org/10.1155/2020/8478016.

Yousefi, S., Derakhshan, F., Karimipour, H., 2020. Applications of big data analytics and machine learning in the internet of things. In: Handbook of Big Data Privacy. Springer International Publishing, Cham, pp. 77–108. https://doi.org/10.1007/978-3-030-38557-6_5.

Zhou, J., Wu, Z., Jiang, Z., Huang, K., Guo, K., Zhao, S., 2022. Background selection schema on deep learning-based classification of dermatological disease. Comput. Biol. Med. 149, 105966 https://doi.org/10.1016/j.compbiomed.2022.105966.

Ziou, D., Nacereddine, N., Goumeidane, A.B., 2021. Scale space Radon transform. IET Image Process. 15, 2097–2111. https://doi.org/10.1049/ipr2.12180.